Research in Astronomy and Astrophysics, 25:075019 (8pp), 2025 July
https://doi.org/10.1088/1674-4527/addb04
CSTR: 32081.14.RAA.addb04

Morphological Study of an Hδ Absorption Line Selected Sample in EGS Field

Shumei Wu[1,2,3], Jia-Sheng Huang[1,3,4], Cheng Cheng[1,3], and Y. Sophia Dai[1,3]

[1] Chinese Academy of Sciences South America Center for Astronomy, National Astronomical Observatories, Chinese Academy of Sciences, Beijing 100101, China; shmwu@nao.cas.cn, jhuang@nao.cas.cn

[2] School of Astronomy and Space Science, University of Chinese Academy of Sciences, Beijing 101408, China

[3] CAS Key Laboratory of Optical Astronomy, National Astronomical Observatories, Chinese Academy of Sciences, Beijing 100101, China

[4] Harvard-Smithsonian Center for Astrophysics, 60 Garden Street, Cambridge, MA 02138, USA

Received 2025 February 24; revised 2025 April 17; accepted 2025 April 22; published 2025 June 17

Abstract

The role of galaxy morphology and stellar population properties in galaxy evolution is crucial for understanding the transition from star-forming to quiescent galaxies. We present an analysis of 94 galaxies with Hδ absorption line equivalent widths greater than 2 Å, selected from the DEEP2 survey EGS field ($0 < z < 1$). The wealth of multi-wavelength coverage enables accurate stellar mass measurements from SED fitting, SFR measurements from UV and MIR, and galaxy population classification based on the *UVJ* diagram. Using HST F814W images, we performed a morphological analysis and found that most galaxies exhibit disk-like structures, with some showing bulge-dominated profiles. The size of our sample is roughly in between the star-forming and quiescent galaxies, implying a transition of galaxy population. We also examined the role of central stellar density (Σ_1) in galaxy evolution and found that galaxies with higher Σ_1 tend to evolve into quiescent galaxies earlier, supporting the "downsizing" scenario. These findings underscore the importance of size, mass, and central density in galaxy evolution.

Key words: galaxies: starburst – galaxies: evolution – galaxies: formation

1. Introduction

Galaxy formation and evolution are largely determined by their star formation activities. However, star-forming in galaxies cannot last forever; otherwise, we would observe much more massive galaxies (Faber et al. 2007; Huang et al. 2013; Ilbert et al. 2013; Xu et al. 2020). Previous research shows that galaxy colors exhibit a bimodality distribution, and the galaxy population can be divided into red sequence and blue cloud in its color-mass diagram (Takamiya et al. 1995; Baldry et al. 2004). It requires a quenching mechanism for a star-forming galaxy to stop its star-forming and transition from the blue cloud to the red sequence to become a quiescent galaxy, as we observe today (Faber et al. 2007). The transition zone from the blue cloud to the red sequence is known as the green valley (Fontana et al. 2004; Glazebrook et al. 2004; Abraham et al. 2007; Arnouts et al. 2007). Star formation quenching is considered to occur in the green valley.

Previous studies of galaxies in the green valley were based on samples selected using ultraviolet (UV)-optical colors (Salim 2014; Schawinski et al. 2014; Estrada-Carpenter et al. 2023). Numerous surveys have produced large spectroscopic or photometric redshift samples (Dressler et al. 1999; Poggianti et al. 1999; Willmer et al. 2006; Lilly et al. 2007; Lilly et al. 2009; Kochanek et al. 2012; Huang et al. 2013; Cheng et al. 2021; Li et al. 2024) to study galaxy populations and their evolution. Several groups (Martin et al. 2007; Wyder et al. 2007; Fang et al. 2013; Salim 2014; Phillipps et al. 2019; Jian et al. 2020) have used colors to select galaxies in the green valley, demonstrating that these galaxies are transitioning from the blue cloud to the red sequence. Mahoro et al. (2019) and Estrada-Carpenter et al. (2023) studied the morphologies of galaxies in the green valley and how they evolve into quiescent galaxies. Wu et al. (2025) proposed a new approach to studying galaxies in the transition zone by using a spectroscopic sample to select galaxies exhibiting Hδ absorption lines in the Balmer sequence. The presence of Balmer absorption lines in galaxy spectra indicates the domination of A-type stars during or after a starburst event. The rising and falling of A-type star fraction in galaxy spectra provide a direct trace of their later-stage evolution, from starburst to quiescent galaxies. Most galaxies selected by the Hδ absorption line method are green-valley galaxies, with a few being post-starburst galaxies in the red sequence.

In this paper, we present a morphological study of a galaxy sample selected based on Hδ absorption lines. The sample was selected from the All-Wavelength Extended Groth Strip International Survey (AEGIS) redshift survey with very extensive multi-wavelength data (Barro et al. 2011). We identified green valley galaxies spectroscopically from the AEGIS redshift sample, enabling a comparison among galaxies in blue-cloud, green-valley, and red sequence zones. There are high-resolution Hubble Space Telescope (HST) and

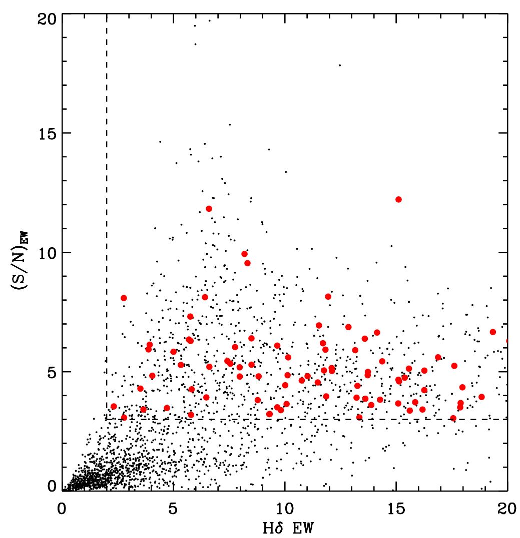

Figure 1. The sample was selected from the EGS field using DEEP2 spectroscopic data. The black dots represent the measurements of Hδ EW for all DEEP2 galaxies. The 94 red dots indicate the final sample selection, which includes galaxies with multi-wavelength photometry (Barro et al. 2011) and F814W imaging. The two lines represent the selection criteria.

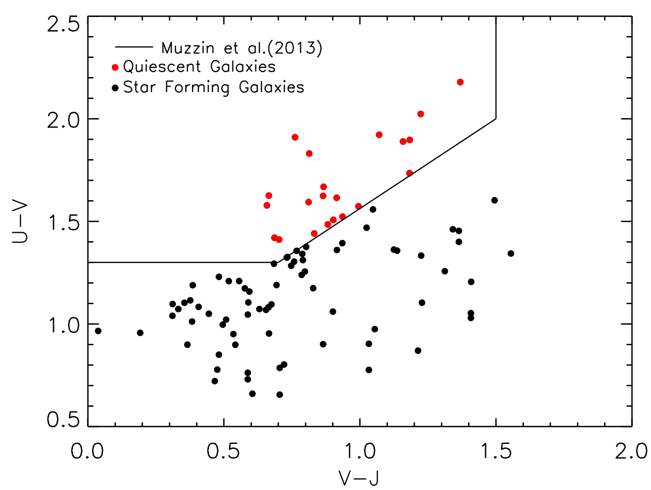

Figure 2. Our sample in the *UVJ* diagram. The passive galaxy criteria are based on Muzzin et al. (2013); 21 galaxies are located in the passive galaxy region, while 73 galaxies lie in the star-forming area of the diagram.

James Webb Space Telescope (JWST) images (Davis et al. 2007; Grogin et al. 2011; Koekemoer et al. 2011; Finkelstein et al. 2023) in the AEGIS survey area, providing well-resolved morphologies for the selected galaxies. We investigated how morphological transformation occurred when the Hδ absorption line selected galaxies evolved from green valley to red sequence.

The structure of this paper is as follows. Section 2 presents a detailed selection of our sample in the AEGIS redshift survey. In Section 3, we measure the physical properties of the sample

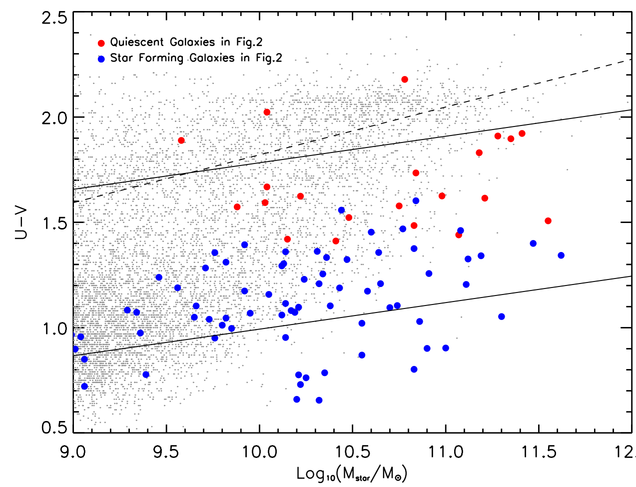

Figure 3. The color-mass diagram. Red and blue dots represent quiescent and star-forming galaxies in our sample, respectively. The gray dots in the background represent galaxies in the CANDELS fields, including those in the EGS. The dashed line separates galaxies in the red sequence and blue cloud, following the criterion from Borch et al. (2006). The two solid lines outline the green valley, as defined by Wang et al. (2017).

and analyze its evolutionary history. Galaxy evolution of the sample traced by A-type stars and their morphologies are also discussed in this section, and we conclude in Section 4. Throughout the paper, we adopt a flat CDM cosmology with $\Omega_M = 0.3$, $\Omega_\Lambda = 0.7$, and $h = 0.7$, and we use the Salpeter initial mass function (IMF, Salpeter 1955) for stellar population modeling.

2. The Hδ Absorption Line Selection

2.1. The Photometric and Spectral Samples in the EGS Field

The Extended Groth Strip (EGS) was one of the four fields in the Deep Extragalactic Evolutionary Probe 2 (DEEP2) survey (Willmer et al. 2006), using the Keck telescopes for spectroscopy and the HST for imaging. The DEEP2 spectroscopic observations covered a red wavelength range (6500–9300 Å) to select galaxies in the redshift range $0.6 < z < 1.2$. We also make use of the MMT/Hectospec archival spectra,[5] which cover a wavelength range of 3900–9240 Å, to complement the observations of targets, especially at $z < 0.6$. The extensive multi-wavelength imaging coverage in the EGS field, spanning from X-ray to radio, makes it a unique data set for studying galaxy evolution, and it became the basis for a survey called the AEGIS; Davis et al. 2007). The full wavelength photometry data, ranging from UV to far-infrared (FIR), enable measurements of stellar mass and star formation rates (SFRs) for galaxies in the AEGIS sample, while X-ray and radio data are used for active galactic nucleus

[5] https://oirsa.cfa.harvard.edu/search/

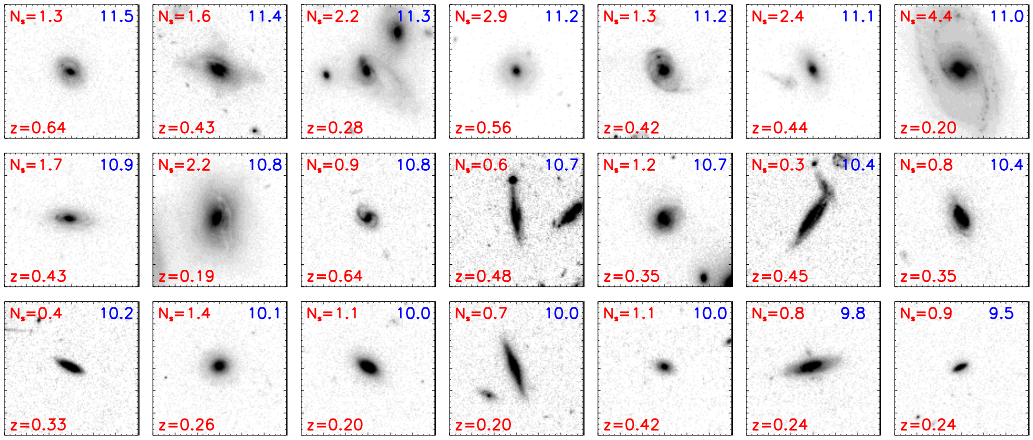

Figure 4. The HST images of the galaxies in the red sequence area of the *UVJ* diagram in Figure 2. Each stamp image size is 20″ × 20″. We provide the $\log(M_*/M_\odot)$, Sérsic index and the redshift at the upper right, upper left and lower right corner of each stamp image respectively.

(AGN) identification. The most critical data for our sample selection in this study are the DEEP2 spectra (Newman et al. 2013) and the HST optical imaging (Davis et al. 2007). More recently, HST and JWST have conducted much deeper imaging surveys in the near-infrared (NIR) and mid-infrared (MIR) bands (Grogin et al. 2011; Koekemoer et al. 2011; Finkelstein et al. 2023), though with much smaller coverage. Our sample selection was based on the measurement of Hδ absorption lines in the DEEP2 spectra. The full optical band spectroscopy in the EGS field allows detection of Hδ absorption lines in the redshift range $0 < z < 1$. The morphological study was performed using the HST F814W images of the EGS field. Barro et al. (2011) provided the multi-wavelength photometry data for the AEGIS survey.

2.2. Hδ Absorption Line Measurement and Sample Selection

We measured the Hδ absorption line equivalent width (EW) for all spectra in the DEEP2 EGS sample with redshifts in the range $0 < z < 1$. At higher redshifts ($z > 1$), the Hδ line shifted out of the spectroscopic range. The detailed measurement method is described in Wu et al. (2025). The Hδ absorption line EW is defined as follows: the nearby continuum is measured in the wavelength ranges $4041.6 < \lambda < 4079.75$ Å and $4128.5 < \lambda < 4161.0$ Å while the absorption line profile is measured in the range $4083.5 < \lambda < 4122.25$ Å. The measurement becomes more complicated when galaxies exhibit both Hδ emission and absorption lines. To address this, we adopted a sophisticated method of iteratively fitting a two-component line. In almost all cases, the absorption line is significantly wider than the emission line. Our method provides robust estimates of the Hδ absorption line EW, even when both emission and absorption lines are present.

For our sample selection, a significant detection of the Hδ absorption line was required. The criteria included both $S/N_{EW} > 3$ and EW > 2 Å to reject poor fitting results, as illustrated in Figure 1. We also added an additional criterion to ensure that the continuum in the wavelength ranges $4041.6 < \lambda < 4079.75$ Å and $4128.5 < \lambda < 4161.0$ Å had at least 5σ significance, which helped reject a substantial number of extremely large EW measurements. A total of 324 galaxies were selected from the area covered by the EGS multi-wavelength photometry. In this project, we aim to study the morphological evolution of starburst galaxies in their last billion years. We further limited our sample to galaxies within the HST F814W imaging coverage in the EGS field. A total of 94 galaxies were selected based on the HST F814W images, with a redshift range of $0 < z < 0.9$.

3. Classification of the Hδ Absorption Line Selected Sample

3.1. Stellar Mass and Star Formation Rate Estimation

The multi-wavelength photometry in the EGS field allows for the estimation of the physical properties of our sample. We fitted the spectral energy distributions (SEDs) using stellar population models (Calzetti et al. 2000; Bruzual & Charlot 2003) and exponentially declining star formation history (SFH) to estimate the stellar mass for each galaxy in the sample. The stellar masses of the galaxies in this sample span a wide range of $8.5 < \log(M_*/M_\odot) < 11.5$. Additionally, we measured the rest-frame $U-V$ and $V-J$ colors for the galaxies. Bimodality classification of the galaxies was performed using the *UVJ* diagram (Figure 2). In Figure 2, 21 galaxies meet the criteria for passive galaxies (Muzzin et al. 2013). The remaining 73 galaxies in the sample are classified as dusty star-forming galaxies. We compared this sample with all galaxies in the CANDELS field at similar redshifts, using the mass-UV-color diagram, and found that most of these galaxies are located in the green valley (Figure 3). As Wu et al. (2025) noted, most of the Hδ-selected galaxies are found either above

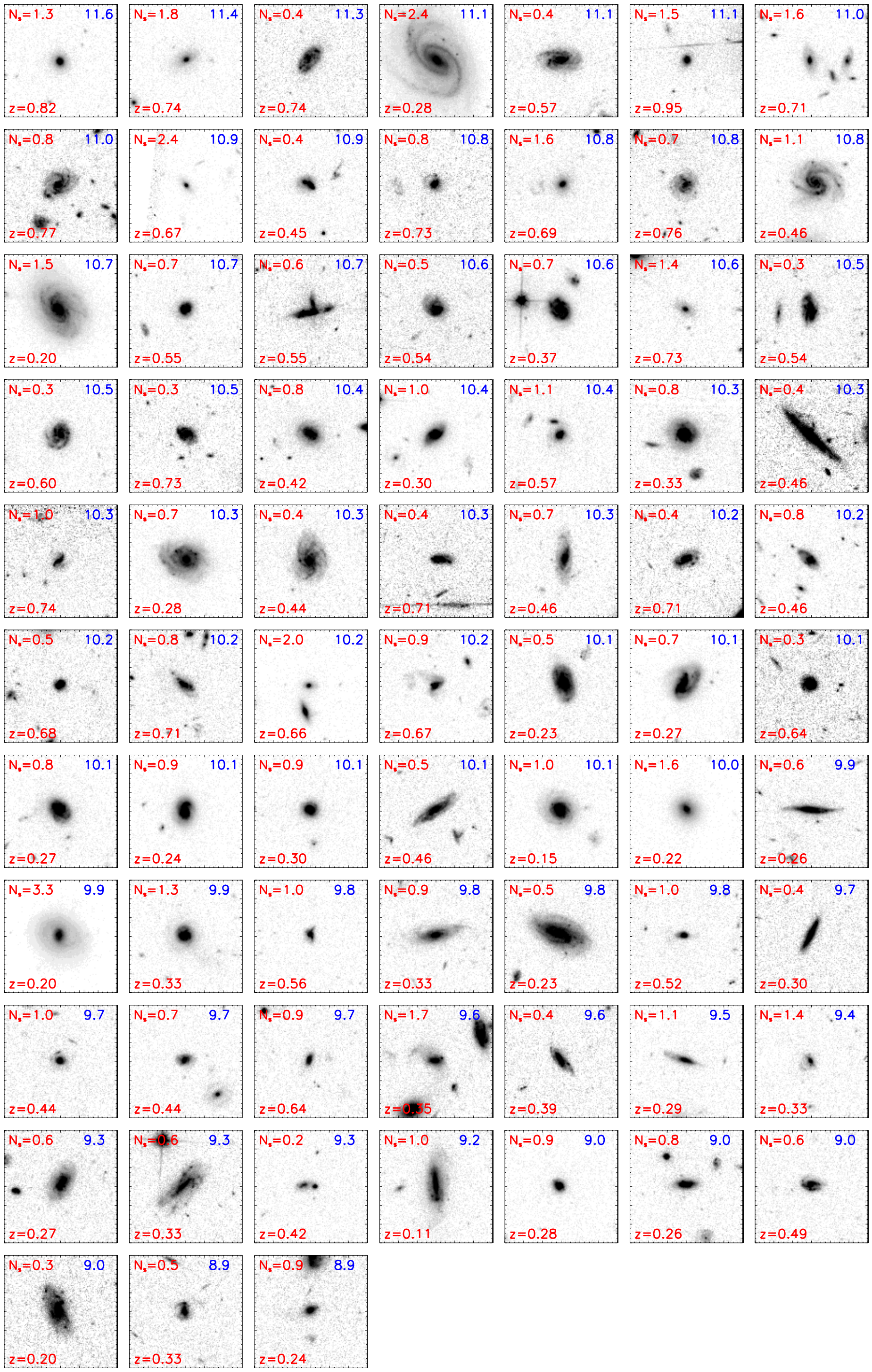

Figure 5. The HST images of the galaxies in the star-forming area of the *UVJ* diagram in Figure 2. The image configuration is the same as Figure 4.

or below the main sequence area. The galaxies in the starburst region are in their later stages, rapidly passing through the main sequence phase to become passive galaxies.

As presented in previous works (Wu et al. 1998; Poggianti et al. 1999; Wu et al. 2025), an Hδ selected sample consists of either starburst or quiescent galaxies. This sample should have a similar SFR distribution. In fact, among the 94 galaxies in this sample, 92 galaxies had the MIPS 24 μm detections including those identified as quiescent galaxies in the *UVJ* diagram. We estimated the total SFRs for galaxies in the sample using both

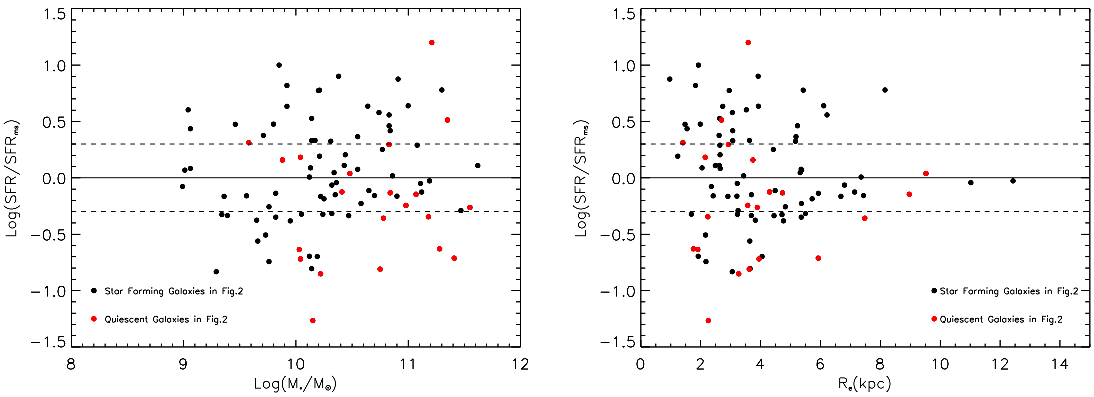

Figure 6. Stellar mass (left panel) and effective radius R_e (right panel) versus SFR normalized by model SFR in the main sequence relation (Popesso et al. 2019). The solid line is the normalized main sequence with the dashed lines defining the main sequence boundary of 0.3 dex above and below it. Wu et al. (2025) found that Hδ-selected galaxy evolution started from the starburst region, passed through the main sequence zone, and became quiescent galaxies. In this study, we found that galaxies with large mass and small size entered the quiescent galaxies earlier.

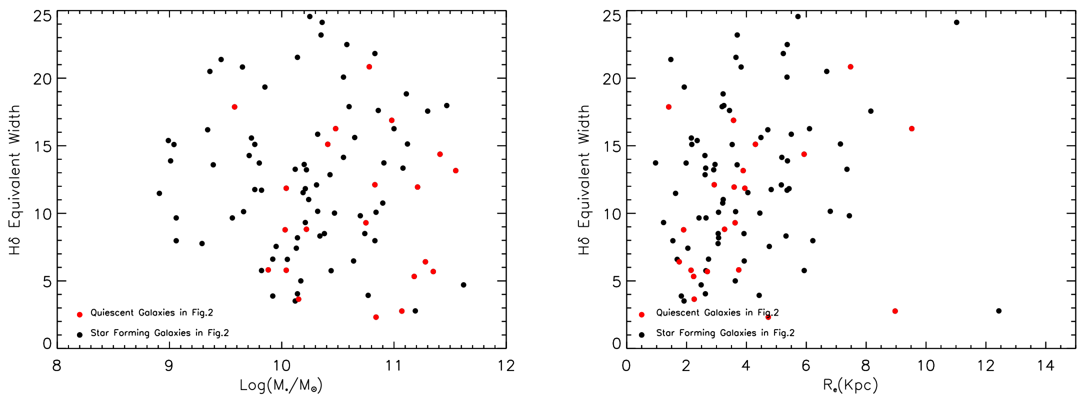

Figure 7. Stellar mass (left panel) and effective radius R_e (right panel) versus Hδ. The right panel shows a rough trend that larger galaxies have deeper Hδ absorption, thus signifying more A-type stars. Yet, galaxies with large Hδ EW appear to have modest stellar mass.

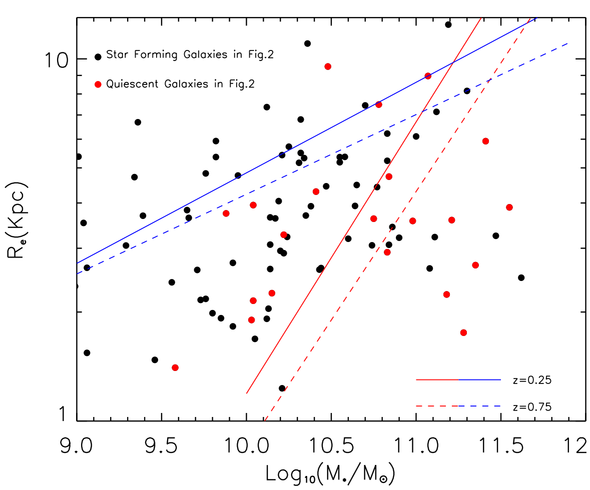

Figure 8. The mass-size distribution for Hδ selected sample. The blue lines represent the mass-size relation for star-forming galaxies, and the red lines represent the relation for quiescent galaxies. Solid and dashed lines correspond to the relations at $z = 0.25$ and $z = 0.75$, respectively (van der Wel et al. 2014). Our sample covers a redshift range of $0.1 < z < 0.9$.

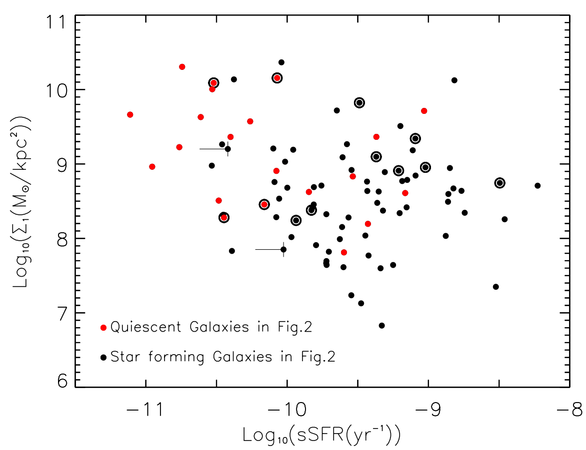

Figure 9. The Σ_1 in this figure is defined in Equation (1). There is an anti-correlation between Σ_1 and sSFR, indicating that galaxies with high densities evolved into quiescent status earlier. We highlight the targets with bright neighbors with circles, and find no clear trend between Σ_1 and the environment.

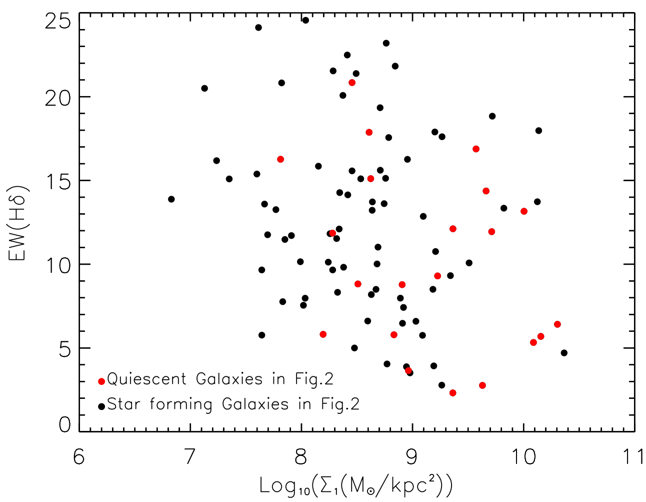

Figure 10. Plot of Hδ EW versus Σ_1 for the Hδ-selected sample. Galaxies with high Σ_1 exhibit smaller Hδ EWs.

UV and IR photometry, following the same method in Wu et al. (2025). The range of SFRs for this sample is $0.1 < \mathrm{SFR} < 100\,M_\odot\,\mathrm{yr}^{-1}$. The specific star formation rate (sSFR), therefore, is in the range of $10^{-12} < \mathrm{sSFR} < 10^{-8}\,\mathrm{yr}^{-1}$. The mean sSFR for quiescent galaxies is Log(sSFR) = −10.3, and that for star-forming galaxies is Log(sSFR) = −9.5.

3.2. Morphological Evolution of the Hδ Selected Sample

We performed morphological analysis for this sample using their HST F814W images. The quiescent galaxy stamp images are presented in Figure 4, and the starburst ones are shown in Figure 5. The galaxies in this sample cover a redshift range of $0.1 < z < 0.9$, so the observed F814W band samples the rest-frame bands of 4000–8000 Å. This wavelength range may not be very sensitive to bulges at $z > 0.6$. A visual inspection shows that most galaxies in the sample are disk or spiral galaxies, with some exhibiting compact morphologies. Notably, typical elliptical galaxies are absent, even among those identified as quiescent galaxies in Figure 2. We used GALFIT (Peng et al. 2002) to fit galaxy profiles in the sample, yielding Sérsic indices and effective radii for each galaxy. Most galaxies have Sérsic indices ∼1, consistent with the visual identification. There are seven galaxies with Sérsic indices >2, five of which are quiescent galaxies, and two are starbursts. All seven galaxies lie in the redshift range of $0.2 < z < 0.6$. Thus, the effective radius R_e is a more robust morphological parameter for this study.

A critical result is that galaxies with different sizes and masses evolve differently in terms of their SFRs and the production of A-type stars. Figure 6 shows that galaxies with large mass and small size cross the main sequence line to become quiescent. This suggests that galaxies with higher densities, rather than simply larger masses, evolve earlier. The Hδ EW for a galaxy varies differently with its mass and size. Figure 7 shows that large Hδ EWs occur in galaxies with modest stellar masses. This is consistent with the simple evolutionary model of Hδ in Couch & Sharples (1987) and Kauffmann et al. (2003), where Hδ increases as the Balmer break strengthens, reaches its peak, and then decreases as the Balmer break continues to increase. As the stellar mass increases with the Balmer break, this explains why very massive galaxies tend to have small Hδ EWs. The peak of the Hδ EW in our sample occurs in galaxies with modest stellar masses. However, Figure 7 also shows that larger galaxies tend to have higher Hδ EWs.

The size-mass relation for this sample is complex. Size-mass relations for different types of galaxies vary significantly. Disk galaxies usually have larger effective radii than those of quiescent galaxies (van der Wel et al. 2014). Sizes for both types of galaxies are correlated with their stellar mass, with the slope for quiescent galaxies being much steeper. Most galaxies in the Hδ selected sample neither follow disk nor quiescent size-mass relation in Figure 8 at similar redshifts, but lie between these relations (van der Wel et al. 2014). Massive galaxies in the sample have rather smaller R_e than most quiescent galaxies in CANDELS (van der Wel et al. 2014).

Another important morphological parameter is the stellar mass surface density within the central 1 kpc radius, known as Σ_1. Cheung et al. (2012) first identified this parameter as a key measure of the galaxy quenching process, which is also strongly related to the central supermassive black hole. Several observational and theoretical studies of galaxies at various redshifts have shown that Σ_1 correlates with stellar mass and can help separate quiescent from star-forming galaxies (Fang et al. 2013; Tacchella et al. 2017; Chen et al. 2020; Estrada-Carpenter et al. 2023; Cattaneo et al. 2025). We used the same Σ_1 equation as Estrada-Carpenter et al. (2023)

$$\Sigma_1 = \frac{\int_0^{1\,\mathrm{kpc}} I(R) 2\pi R dR}{\int_0^{\infty} I(R) 2\pi R dr} \frac{M_*}{\pi\,(1\,\mathrm{kpc})^2}, \tag{1}$$

in which

$$I(R) = I_e \exp\left(-b_n\left[\left(\frac{R}{R_e}\right)^{1/n} - 1\right]\right), \tag{2}$$

and show the results in Figures 9, 10 and 11.

Our results show that the Σ_1 for galaxies in the sample is correlated with their stellar mass (Figure 11). However, only a few massive galaxies fall above the quiescent galaxy boundary, consistent with their lower sSFRs in Figure 9. Figures 10 and 11 also show that quiescent galaxies tend to have small Hδ absorption, indicating a lower fraction of A-type stars in these galaxies. From Figures 4 and 5, we see that some targets have bright neighbors or are located in denser environments, which may lead to a more compact stellar

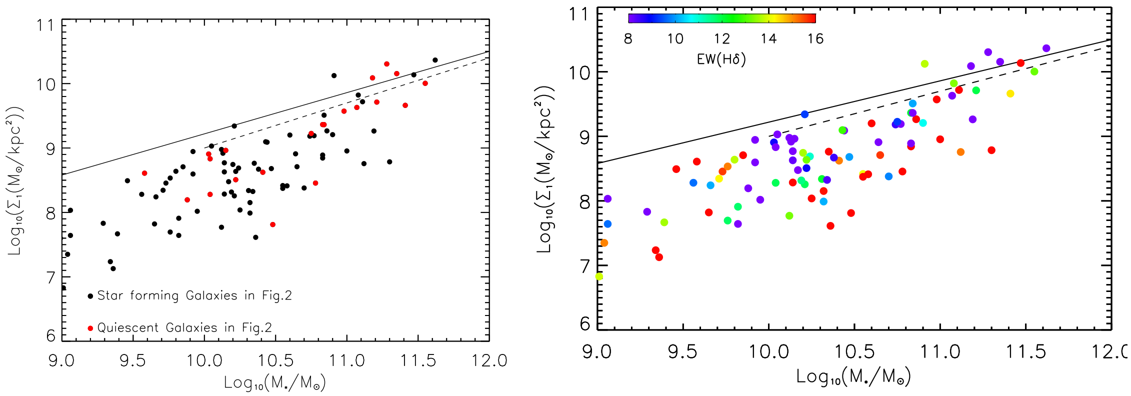

Figure 11. Σ_1 versus stellar mass M^* for the sample. The correlation between these two parameters is known to be tighter for both star-forming and quiescent galaxies (Cheung et al. 2012; Fang et al. 2013; Chen et al. 2020). The solid lines represents the fit of the Σ_1–stellar mass relation for quiescent Sloan Digital Sky Survey (SDSS) galaxies (Tacchella et al. 2017). The dashed lines marks the boundary for quiescent galaxies at $0.5 < z < 1$, as described in Chen et al. (2020). The right panel shows the distribution of Hδ EWs along the Σ_1–M^* relation.

surface density and a higher Σ_1 value. We highlight these targets in Figure 9 and find no clear trend between environment and central stellar mass density Σ_1.

In previous studies (Cowie et al. 1996; Heavens et al. 2004; Thomas et al. 2005), galaxy evolution exhibits a "downsizing" effect in which massive galaxies evolve to become quiescent galaxies earlier. Current studies (including this one) show that galaxies with high Σ_1 evolve earlier. The correlation between Σ_1 and stellar mass makes it indistinguishable. Tacchella et al. (2017) and Chen et al. (2020) studied galaxy populations at various redshifts, and found that in each redshift bin both star-forming and quiescent galaxies can have the same Σ_1 in their Σ_1–M_* plots. This suggests an evolutionary scenario in which a galaxy can evolve across the line to become a quiescent galaxy by increasing its central density Σ_1. Galaxies in our Hδ selected sample do not show a similar distribution in Figure 11, where star-forming galaxies below the boundary line at the lower mass end and quiescent galaxies lie above the boundary line. This may not be consistent with the scenario of galaxy evolution in the vertical direction in the Σ_1–M_* diagram, but rather with galaxies with high Σ_1 that evolved earlier.

4. Summary

We investigate a sample of galaxies with Hδ absorption line EWs > 2 from the DEEP2 survey EGS field ($0 < z < 1$). We selected 94 galaxies based on robust Hδ detection and HST F814W coverage, which were used for morphological analysis. Stellar masses in this sample range from $8.5 < \log(M_*/M_\odot) < 11.5$, with SFRs spanning 0.1–100 $M_\odot$ yr^{-1}. Based on their *UVJ* colors, we classified the galaxies as quiescent or star-forming.

The morphological analysis revealed that most galaxies in our Hδ EW selected sample have disk-like structures, while a few show bulge-dominated profiles. The half light radii of our sample lie between the star-forming and quiescent galaxy sample, indicating a transition nature of our sample. We found that galaxies with higher central densities (Σ_1) tend to evolve into quiescent galaxies earlier. These results suggest that galaxy evolution is strongly influenced by central density, with galaxies exhibiting high Σ_1 evolving more rapidly, supporting the "downsizing" effect. This study highlights the importance of galaxy size, mass, and central density in shaping their evolutionary paths.

Acknowledgments

We thank the referee for careful reading and helpful comments. This work is sponsored by the National Key R&D Program of China for grant No. 2022YFA1605300, and the National Natural Science Foundation of China (NSFC, Grant Nos. 11933003, 12173045, and 12273051). Additional support came from the Chinese Academy of Sciences (CAS) through a grant to the South America Center for Astronomy (CASSACA) in Santiago, Chile. C.C. is supported by Chinese Academy of Sciences South America Center for Astronomy (CASSACA) Key Research Project E52H540301.

ORCID iDs

Shumei Wu https://orcid.org/0009-0008-9984-1681

References

Abraham, R. G., Nair, P., McCarthy, P. J., et al. 2007, ApJ, 669, 184
Arnouts, S., Walcher, C. J., Le Fèvre, O., et al. 2007, A&A, 476, 137
Baldry, I. K., Glazebrook, K., Brinkmann, J., et al. 2004, ApJ, 600, 681
Barro, G., Pérez-González, P. G., Gallego, J., et al. 2011, ApJS, 193, 13
Borch, A., Meisenheimer, K., Bell, E. F., et al. 2006, A&A, 453, 869
Bruzual, G., & Charlot, S. 2003, MNRAS, 344, 1000
Calzetti, D., Armus, L., Bohlin, R. C., et al. 2000, ApJ, 533, 682
Cattaneo, A., Dimauro, P., & Koutsouridou, I. 2025, MNRAS, 537, 3929
Chen, Z., Faber, S. M., Koo, D. C., et al. 2020, ApJ, 897, 102
Cheng, C., Huang, J.-S., Willmer, C. N. A., et al. 2021, ApJS, 256, 4

Cheung, E., Faber, S. M., Koo, D. C., et al. 2012, ApJ, 760, 131
Couch, W. J., & Sharples, R. M. 1987, MNRAS, 229, 423
Cowie, L. L., Songaila, A., Hu, E. M., & Cohen, J. G. 1996, AJ, 112, 839
Davis, M., Guhathakurta, P., Konidaris, N. P., et al. 2007, ApJL, 660, L1
Dressler, A., Smail, I., Poggianti, B. M., et al. 1999, ApJS, 122, 51
Estrada-Carpenter, V., Papovich, C., Momcheva, I., et al. 2023, ApJ, 951, 115
Faber, S. M., Willmer, C. N. A., Wolf, C., et al. 2007, ApJ, 665, 265
Fang, J. J., Faber, S. M., Koo, D. C., & Dekel, A. 2013, ApJ, 776, 63
Finkelstein, S. L., Bagley, M. B., Ferguson, H. C., et al. 2023, ApJL, 946, L13
Fontana, A., Pozzetti, L., Donnarumma, I., et al. 2004, A&A, 424, 23
Glazebrook, K., Tober, J., Thomson, S., Bland-Hawthorn, J., & Abraham, R. 2004, AJ, 128, 2652
Grogin, N. A., Kocevski, D. D., Faber, S. M., et al. 2011, ApJS, 197, 35
Heavens, A., Panter, B., Jimenez, R., & Dunlop, J. 2004, Natur, 428, 625
Huang, J. S., Faber, S. M., Willmer, C. N. A., et al. 2013, ApJ, 766, 21
Ilbert, O., McCracken, H. J., Le Fèvre, O., et al. 2013, A&A, 556, A55
Jian, H.-Y., Lin, L., Koyama, Y., et al. 2020, ApJ, 894, 125
Kauffmann, G., Heckman, T. M., White, S. D. M., et al. 2003, MNRAS, 341, 33
Kochanek, C. S., Eisenstein, D. J., Cool, R. J., et al. 2012, ApJS, 200, 8
Koekemoer, A. M., Faber, S. M., Ferguson, H. C., et al. 2011, ApJS, 197, 36
Li, Z.-J., Dai, Y. S., Huang, J. S., Wuyts, S., & Cao, T.-W. 2024, ApJ, 963, 99
Lilly, S. J., Le Brun, V., Maier, C., et al. 2009, ApJS, 184, 218
Lilly, S. J., Le Fèvre, O., Renzini, A., et al. 2007, ApJS, 172, 70
Mahoro, A., Pović, M., Nkundabakura, P., Nyiransengiyumva, B., & Väisänen, P. 2019, MNRAS, 485, 452
Martin, D. C., Wyder, T. K., Schiminovich, D., et al. 2007, ApJS, 173, 342
Muzzin, A., Marchesini, D., Stefanon, M., et al. 2013, ApJ, 777, 18
Newman, J. A., Cooper, M. C., Davis, M., et al. 2013, ApJS, 208, 5
Peng, C. Y., Ho, L. C., Impey, C. D., & Rix, H.-W. 2002, AJ, 124, 266
Phillipps, S., Bremer, M. N., Hopkins, A. M., et al. 2019, MNRAS, 485, 5559
Poggianti, B. M., Smail, I., Dressler, A., et al. 1999, ApJ, 518, 576
Popesso, P., Concas, A., Morselli, L., et al. 2019, MNRAS, 483, 3213
Salim, S. 2014, SerAJ, 189, 1
Salpeter, E. E. 1955, ApJ, 121, 161
Schawinski, K., Urry, C. M., Simmons, B. D., et al. 2014, MNRAS, 440, 889
Tacchella, S., Carollo, C. M., Faber, S. M., et al. 2017, ApJL, 844, L1
Takamiya, M., Kron, R. G., & Kron, G. E. 1995, AJ, 110, 1083
Thomas, D., Maraston, C., Bender, R., & Mendes de Oliveira, C. 2005, ApJ, 621, 673
van der Wel, A., Franx, M., van Dokkum, P. G., et al. 2014, ApJ, 788, 28
Wang, T., Elbaz, D., Alexander, D. M., et al. 2017, A&A, 601, A63
Willmer, C. N. A., Faber, S. M., Koo, D. C., et al. 2006, ApJ, 647, 853
Wu, H., Zou, Z. L., Xia, X. Y., & Deng, Z. G. 1998, A&AS, 132, 181
Wu, S., Huang, J.-S., Cheng, C., & Dai, Y. S. 2025, ApJ, 980, 192
Wyder, T. K., Martin, D. C., Schiminovich, D., et al. 2007, ApJS, 173, 293
Xu, H., Dai, Y. S., Huang, J.-S., et al. 2020, ApJ, 905, 103